HHS Public Access

Author manuscript

Oncogene. Author manuscript; available in PMC 2015 January 03.

Published in final edited form as:

Oncogene. 2014 July 3; 33(27): 3571–3582. doi:10.1038/onc.2013.320.

LIM Domain Kinases as Potential Therapeutic Targets for Neurofibromatosis Type 2

Alejandra Petrilli, M.S., M.S.[1], **Alicja Copik, Ph.D.**[1], **Michelle Posadas, B.S.**[1], **Long-Sheng Chang, Ph.D.**[2,3], **D. Bradley Welling, M.D., Ph.D.**[4], **Marco Giovannini, M.D., Ph.D.**[5], and **Cristina Fernández-Valle, Ph.D.**[1]

[1]Department of Biomedical Science, College of Medicine, University of Central Florida, Orlando, FL 32827, USA

[2]Center for Childhood Cancer, The Research Institute at Nationwide Children's Hospital, The Ohio State University College of Medicine, Columbus, OH 43205, USA

[3]Department of Pediatrics, The Ohio State University College of Medicine, Columbus, OH 43205, USA

[4]Department of Otolaryngology, The Ohio State University College of Medicine, Columbus, OH 43205, USA

[5]House Research Institute, Division of Clinical and Translational Research, Los Angeles, CA 90057, USA

Abstract

Neurofibromatosis Type 2 (NF2) is caused by mutations in the *neurofibromatosis 2* (*NF2*) gene that encodes a tumor suppressor protein called merlin. NF2 is characterized by formation of multiple schwannomas, meningiomas and ependymomas. Merlin loss of function is associated with increased activity of Rac and p21-activated kinases (PAK) and deregulation of cytoskeletal organization. LIM domain kinases (LIMK1 and 2) are substrate for Cdc42/Rac-PAK, and modulate actin dynamics by phosphorylating cofilin at serine-3. This modification inactivates cofilin's actin severing and depolymerizing activity. LIMKs also translocate into the nucleus and regulate cell cycle progression. Significantly, LIMKs are overexpressed in several tumor types, including skin, breast, lung, liver and prostate. Here we report that mouse Schwann cells (MSCs) in which merlin function is lost as a result of *Nf2* exon2 deletion ($Nf2^{\Delta Ex2}$) exhibited increased levels of LIMK1, LIMK2, and active phospho-Thr508/505-LIMK1/2, as well as phospho-Ser3-cofilin, compared to wild-type normal MSCs. Similarly, levels of LIMK1 and 2 total protein and active phosphorylated forms were elevated in human vestibular schwannomas compared to normal human Schwann cells (SCs). Reintroduction of wild-type *NF2* into $Nf2^{\Delta Ex2}$ MSC reduced LIMK1

Corresponding author: Cristina Fernández-Valle, Ph.D., Burnett School of Biomedical Sciences, College of Medicine, University of Central Florida, 6900 Lake Nona Blvd., Orlando, FL 32827, U.S.A., cfv@ucf.edu, Phone: 407-266-7033, fax: 407-266-7002.

Conflict of interest

The authors declare no conflicts of interest.

Supplementary Information accompanies the paper on the Oncogene website http://www.nature.com/onc

and LIMK2 levels. We show that pharmacological inhibition of LIMK with BMS-5, decreased the viability of *Nf2*$^{\Delta Ex2}$ MSCs in a dose-dependent manner, but did not affect viability of control MSCs. Similarly, LIMK knockdown decreased viability of *Nf2*$^{\Delta Ex2}$ MSCs. The decreased viability of *Nf2*$^{\Delta Ex2}$ MSCs was not due to caspase-dependent or -independent apoptosis, but rather, to inhibition of cell cycle progression as evidenced by accumulation of cells in G_2/M phase. Inhibition of LIMKs arrest cells in early mitosis by decreasing Aurora A activation. Our results suggest that LIMKs are potential drug targets for NF2 and tumors associated with merlin deficiency.

Keywords

LIMK; cell proliferation; Neurofibromatosis; schwannomas; cytoskeleton dynamics; cell cycle

Introduction

Mutations in the tumor suppressor gene *NF2* cause neurofibromatosis type 2 (NF2), an autosomal dominant disorder with an incidence of about one in 25,000 individuals [(1)]. The characteristic feature of NF2 is the development of bilateral vestibular schwannomas that typically cause deafness, facial paralysis and disequilibrium following surgical removal to prevent life-threatening complications. Frequently, NF2 patients also develop multiple schwannomas in other nerves as well as meningiomas and ependymomas [(2)]. Mutations in the *NF2* gene are also common in malignant mesothelioma [(3)]. Currently, the standard treatment for NF2 schwannomas is microsurgery or stereotactic radiosurgery. Unfortunately, limited operability, poor preservation of hearing, diminished functionality of facial nerves and the small risk of radiation-induced malignant transformation later, compromise good clinical outcomes. Only a handful of NF2 pre-clinical and clinical trials are ongoing, all of which utilize existing anti-cancer drugs [(4, 5)].

The *NF2* gene encodes a tumor suppressor called merlin or schwannomin. Merlin regulates a number of processes in Schwann cells (SCs) [(6, 7)]. Normal SCs usually proliferate slowly and adopt a bipolar morphology, however, merlin-deficient human schwannoma cells exhibit abnormalities in proliferation, motility and morphology *in vitro*[(8)]. Merlin's mechanism of action remains poorly understood, but appears to involve regulation of surface receptor activity and turnover by modulation of their interactions with the actin cytoskeleton and transduction of downstream signals [(7)]. A potential pathway through which merlin regulates the actin cytoskeleton involves Cdc42/Rac-PAK-LIMK-cofilin [(9–11)]. Loss of merlin function is associated with elevated levels of active Rac and p21-activated kinase (PAK), suggesting that merlin is a negative regulator of Rac and PAK-dependent pathways. Conversely, PAK phosphorylates and inactivates merlin's tumor suppressor activity [(12, 13)]. Work from our laboratory has shown that activation of β1-integrin in normal SCs promotes PAK-dependent phosphorylation of merlin at serine-518 (ref.14). While PAK has been studied as a potential therapeutic target for NF2, its large number of substrates confounds its usefulness [(15)].

The LIM kinase (LIMK) family has two members, LIMK1 and LIMK2, which can be phosphorylated by Cdc42/Rac-PAK1, 2 and 4 at threonine-505/508 and converted into active serine/threonine kinases. LIMKs are also regulated by Rho-associated kinases (ROCK) and the myotonic dystrophy kinase-related Cdc42-binding kinase (MRCK). The major LIMK substrate is the actin depolymerizing and severing protein cofilin/ADF [16]. LIMK-dependent phosphorylation of cofilin at serine-3 inactivates cofilin and promotes stabilization of the actin cytoskeleton [17]. LIMKs also translocate from the cortical cytoplasm and focal adhesions, where they modulate cell morphology and motility, to the centrosome and nucleus, where they regulate mitosis and cytokinesis [18–24]. LIMKs interact with Aurora A, a serine/threonine kinase involved in centrosome dynamics, spindle assembly and chromosome alignment and segregation during mitosis [25, 26].

Aurora A is found on duplicated centrosomes and mitotic spindle microtubules. During early mitosis phospho-LIMKs co-localize with γ-tubulin in the centrosomes. In metaphase LIMK1 is found at the spindle poles and later redistributes to the cleavage furrow. LIMK2 is located along the spindle and at the cleavage furrow of post-mitotic cells. LIMK1 is a substrate for, and phosphorylates Aurora A to promote its autophosphorylation at Thr288 (ref.27). LIMK2 is an Aurora A substrate and stabilizes it by kinase and scaffolding actions [28]. LIMKs are overexpressed and implicated in various cancers, such as breast, lung, skin, liver and prostate, and several tumor cell lines [29–32]. Hence, LIMKs are emerging cancer targets yet, few inhibitors have been identified [33].

We show that the levels of total and phosphorylated LIMK and its phosphorylated substrate are elevated in sporadic vestibular schwannomas (VS) compared to normal human SCs. Utilizing *Nf2*$^{\Delta Ex2}$ mouse Schwann cells (MSCs) as a cellular model of NF2, we show that pharmacological inhibition or genetic silencing of LIMK significantly reduces proliferation of *Nf2*$^{\Delta Ex2}$ MSCs, but does not substantially affect control *Nf2*$^{flox2/flox2}$ MSCs. The decreased proliferation is due to cell cycle arrest in the G_2/M phase. Pharmacological inhibition of LIMKs with BMS-5 slows mitotic progression by decreasing phosphorylation of cofilin and Aurora A. These studies suggest that LIMKs are potential therapeutic targets for NF2 and other merlin-deficient tumors.

Results

LIMK and phospho-cofilin levels are elevated in Nf2$^{\Delta\ Ex2}$ MSCs compared to controls

Using two complementary techniques, we assessed the levels of LIMK and phospho-Ser3-cofilin in *Nf2*- deficient (*Nf2*$^{\Delta Ex2}$) MSC lines developed by *in vitro* ad-Cre deletion of *Nf2* exon2 from *Nf2*$^{flox2/flox2}$ MSCs [34]. By immunostaining *Nf2*$^{\Delta Ex2}$ MSCs were confirmed to be merlin-deficient and expressed the SC marker S100 (Figure 1a). Merlin-deficient Schwann cells were larger than control *Nf2*$^{flox2/flox2}$ MSCs and had increased levels of F-actin revealed by phalloidin staining. The intensity of LIMK1 and LIMK2 immunofluorescence was higher in *Nf2*$^{\Delta Ex2}$ MSCs than in controls and was detected throughout the cell. Consistent with increased LIMK activity, the intensity of phospho-Ser3-cofilin immunofluorescence was also higher in *Nf2*$^{\Delta Ex2}$ MSCs than in controls (Figure 1 a, b).

We also assessed merlin expression in control $Nf2^{flox2/flox2}$ and $Nf2^{\Delta Ex2}$ MSCs by western blotting using an N-terminal merlin antibody. Merlin was detected in $Nf2^{flox2/flox2}$ MSCs but not in $Nf2^{\Delta Ex2}$ MSCs (Figure 1 c). The status of the *Nf2* gene was also confirmed by PCR analysis of DNA and revealed deletion of exon 2 in $Nf2^{\Delta Ex2}$ as evidenced by a 338-bp band (Figure 1 d) [34].

In addition, western blotting confirmed that levels of both LIMK1 and LIMK2 protein were higher in $Nf2^{\Delta Ex2}$ MSCs than in $Nf2^{flox2/flox2}$ MSCs (Figure 1 e). We detected a coordinate increase in the level of phospho-Ser3-cofilin in $Nf2^{\Delta Ex2}$ MSCs with respect to control consistent with high levels of LIMK activity (Figure 1 f).

Reintroduction of wild-type NF2 normalizes LIMK protein levels

To assess whether elevated LIMK levels were linked to merlin inactivation, we reintroduced a halo-tagged wild-type human *NF2* into $Nf2^{\Delta Ex2}$ MSCs by nucleofection. This method yielded ~10% transfection rate, determined by halo-tag fluorescence labeling. Re-expression of merlin in cultured $Nf2^{\Delta Ex2}$ MSCs generally decreased LIMK1, LIMK2 and phospho-Ser3-cofilin levels (Figure 2 a, b). This result supports a relationship between merlin inactivation and increased LIMK expression and activity.

Pharmacological inhibition of LIMK1/2 by BMS-5 or genetic silencing of LIMK1/2 reduces $Nf2^{\Delta Ex2}$ MSC viability

We next sought to determine whether LIMK was a potential drug target for NF2. We tested the efficacy of BMS-5, a highly selective small molecule inhibitor of LIMK1/2, on reducing phosphorylation of cofilin on Ser3 (ref. 35). BMS-5 inhibited cofilin-Ser3 phosphorylation in a dose-dependent manner in $Nf2^{\Delta Ex2}$ MSCs with an IC_{50} of ~ 2 μM (Figure 3 a, b). We next tested the ability of BMS-5 to reduce viability of $Nf2^{\Delta Ex2}$ MSCs. The 100% viability control was 0.1% DMSO and a positive cell death control was obtained with 50 μM rapamycin (RM) that caused approximately 80% cell death in 24 hours. BMS-5 reduced $Nf2^{\Delta Ex2}$ MSC viability in a dose-dependent manner with an IC_{50} of 3.9 μM (Figure 3 c), but did not significantly reduce the viability of control $Nf2^{flox2/flox2}$ MSCs at equivalent BMS-5 concentrations (Figure 3 d). At 10μM BMS-5, $Nf2^{\Delta Ex2}$ MSC viability was 40% compared to 83% for controls.

To confirm the validity of LIMK as a drug target, we knocked down LIMK1 and LIMK2 in $Nf2^{\Delta Ex2}$ MSCs using lentiviral shRNA transduction (Supplementary Figure S1). Consistent with the BMS-5 results, LIMK1 and LIMK2 knockdown reduced viability of $Nf2^{\Delta Ex2}$ MSCs compared to scrambled shRNA controls in a 24 hour assay (Figure 3 e). These results suggest that LIMK inhibition or silencing in merlin-deficient cells reduces their viability either by promoting cell death or hindering proliferation.

Decreased viability of $Nf2^{\Delta Ex2}$ MSCs in response to BMS-5 or LIMK silencing is independent of apoptosis

To determine if BMS-5 promoted $Nf2^{\Delta Ex2}$ MSCs apoptosis, we measured caspase 3/7 activity. We found that BMS-5 did not activate caspase3/7, whereas the positive control, staurosporine, promoted dose-dependent activation of caspase 3/7 (Figure 5 a). To determine

if BMS-5 promoted caspase-independent apoptosis, we analyzed BMS-5-treated *Nf2*$^{\Delta Ex2}$ MSCs by flow cytometry using a ratiometric membrane asymmetry probe that detects loss of membrane phospholipid asymmetry associated with apoptosis. We observed only a small increase (3.5%) of apoptotic cells after 7 hours of BMS-5 treatment (Figure 4 b). Consistent with pharmacological LIMK inhibition, knockdown of LIMK1 or LIMK2 was not associated with caspase 3/7 activity increase compared to scrambled shRNA controls examined 24 hours after plating (Figure 4 c). Similarly, caspase-independent apoptosis was not observed in *Nf2*$^{\Delta Ex2}$ MSCs transduced with either LIMK1 or LIMK2 shRNA (Figure 4 d). These results suggest that pharmacological inhibition and genetic silencing of LIMK affect *Nf2*$^{\Delta Ex2}$ MSC viability through an apoptosis-independent mechanism.

Pharmacological inhibition of LIMK1/2 by BMS-5 reduces DNA synthesis and cell-cycle progression

We next assessed the ability of BMS-5 to interfere with proliferation of *Nf2*$^{\Delta Ex2}$ MSCs. The cells were incubated with 1 and 2 μM BMS-5 for 24, 48 and 72 hours and cell numbers were measured using crystal violet staining. We observed fewer BMS-5 treated *Nf2*$^{\Delta Ex2}$ MSCs than DMSO-treated controls (Figure 5 a). In addition, we found that BMS-5 decreased DNA synthesis in *Nf2*$^{\Delta Ex2}$ MSCs in a dose-dependent manner (Figure 5 b).

To test the possibility that the decrease in proliferation was a consequence of cell-cycle inhibition, we performed flow cytometry analysis of cells stained with propidium iodine (PI). BMS-5 interfered with *Nf2*$^{\Delta Ex2}$ MSCs cell-cycle progression as evidenced by an increase in the percentage of diploid cells trapped in the G_2/M phase (Figure 6 a). We further analyzed the distribution of cells among the cell-cycle phases using a BrdU/7AAD assay. There was a significant increase in the number of cells accumulating in the G_2/M phase in samples treated with 5 μM BMS-5 as compared to vehicle control (20% vs. 42%). This was accompanied by a decrease in the number of BMS-5 treated cells in G_1 as compared to control (41% vs. 26%). This is consistent with the results obtained by analysis of PI staining (Figure 6 b–c). Overlay of the 7AAD-area histograms clearly demonstrated a significant increase in the G_2/M population in BMS-5 compared to DMSO treated cells (Figure 6 d). Furthermore, the increase in the G_2/M population was accompanied by an increase in the number of cells with higher DNA content consistent with a polyploidy or multinucleated cell population. There was also a smaller but substantial change in number of cells detected in the S-phase of cell cycle in samples treated with BMS-5 as compared to DMSO control. Lastly, the population of cells in the S phase decreased with increasing BMS-5 concentration (Supplementary Figure S2). These results taken together suggest that inhibition of LIMK activity in *Nf2*$^{\Delta Ex2}$ MSCs interferes with progression of the G2/M phase of the cell cycle, thereby decreasing the number of viable *Nf2*$^{\Delta Ex2}$ MSCs.

BMS-5 inhibition of LIMK1/2 activity decreases Aurora A phosphorylation and causes formation of abnormal mitotic spindles

To identify additional down-stream effects of BMS-5 (beyond inhibition of cofilin-Ser3 phosphorylation) that could cause a G_2/M arrest, we tested the levels of Aurora A phosphorylation. Aurora A interacts with both LIMK1 and 2 and is a major regulator of mitotic spindle assembly and chromosomal alignment and segregation. We found that

Nf2$^{\Delta Ex2}$ MSCs treated with increasing concentrations of BMS-5 had a dose dependent decrease phosphorylation of Aurora A at Thr288 (Figure 7 a, b).

We next studied the effect of BMS-5 on the spindle assembly visualizing the mitotic nuclei and spindle machinery by immunostaining. We found that *Nf2*$^{\Delta Ex2}$ MSCs had normal spindle assembly and BMS-5 treated *Nf2*$^{\Delta Ex2}$ MSCs showed abnormal spindle structure (Figure 8 a). Analyzing the centrosome positioning by immunostaining for centrin-1, we found that BMS-5 treated cells were not able to organize the centrosomes and generally had more than two with different sizes (Figure 8 b). We conducted cell cycle analysis and found that the percentage of cells in late G_2/M, visualized by positive immunostaining for the mitotic marker phospho-Ser10-histone3 (pH3), significantly increased from 5% to 17% in the BMS-5 treated *Nf2*$^{\Delta Ex2}$ MSCs compared to DMSO controls (Figure 8 c, d). We observed a highly significant decrease in the percentage BMS-5 treated *Nf2*$^{\Delta Ex2}$ MSCs that advanced to late mitotic phases (anaphase/telophase). Moreover, BMS-5 treated *Nf2*$^{\Delta Ex2}$ MSCs had abnormal spindles and chromosomes did not align at the center as occurs in metaphase (Figure 8 a–e). These results suggest that LIMK inhibition exerts its anti-proliferative effect not only by altering organization of the actin cytoskeleton through inhibition of cofilin phosphorylation but also by decreasing LIMK dependent activation of Aurora A.

LIMKs levels are elevated in representative samples of human vestibular Schwannoma compared to human SCs

To examine the relevance of LIMK inhibition to NF2, we compared LIMK1 and LIMK2 protein and phosphorylation levels in a small number of samples of HSCs from normal individuals and sporadic human vestibular schwannomas (VSs). We observed a significant increase ($P<0.05$ determined using unpaired *t*- test of HSC vs. VS populations, two-tailed) in both the protein and phospho-Thre508 levels of LIMK1 in VSs compared to HSCs (Figure 9a, b). Similarly, both LIMK2 and phospho-Thr505-LIMK2 levels showed a tendency to be higher in VSs compared to HSCs (Figure 9 c, d). Interestingly, the proportion of phospho-Ser3-cofilin to the total cofilin was higher in VSs than in HSCs (Figure 9 e).

We also measured LIMK protein and phosphorylation levels in a human schwannoma cell line, HEI-193, developed from a NF2 patient by immortalization with HPV E6-E7 genes[36]. Although the phospho-Thr508/Thr505 LIMK1/2 antibody recognized multiple bands, the relative intensities of the most prominent phospho-LIMK 1/2 (Thr508/Thr505) bands were also higher in HEI-193 cells than in control HSCs (Figure 9 f).

Discussion

LIMK expression and activity are elevated in merlin-deficient SCs compared to normal SCs

Here we document an association between loss of merlin function and increased levels of LIMK1 and LIMK2 expression and activity. The increased LIMK activity in *Nf2*-deficient MSCs is consistent with its activation by Cdc42/Rac-PAK1, 2 and 4 (ref.16), which have been well-documented to be increased in schwannomas [12, 15]. Importantly, reintroduction of merlin into *Nf2*$^{\Delta Ex2}$ MSCs reduced LIMK and phospho-Ser3-cofilin levels, further supporting an association between loss of merlin function and inactivation of cofilin's actin-

severing and depolymerizing activity downstream of activation of the Rac/PAK/LIMK pathway. In agreement with previous studies of human schwannoma cells, we found that *Nf2*$^{\Delta Ex2}$ MSCs exhibited an abnormal actin cytoskeleton compared to control MSCs [8]. Interestingly, similar cytoskeleton characteristics, indicative of F-actin stabilization, have been reported in C2C12 and HeLa cells overexpressing LIMK [17, 37]. We propose that phosphorylation and inactivation of cofilin downstream of elevated Rac/PAK/LIMK activity could account for the reported increased cell size and abundance of actin filaments observed in *Nf2*$^{\Delta Ex2}$ MSCs and human schwannoma cells [38].

Inhibition of LIMK activities causes cell-cycle arrest of Nf2$^{\Delta Ex2}$ MSCs by preventing Aurora A activation

We recently demonstrated using BMS-5 that LIMK-dependent phosphorylation of cofilin is necessary for stable alignment of SC processes along sensory neuron axons in culture[39]. Here we showed that BMS-5 decreased *Nf2*-deficient MSCs viability in a dose-dependent manner while having little effect on controls. These results suggest a potential therapeutic window for treatment of schwannomas with LIMK inhibitors. Studies using shRNA knockdown of LIMK1 and LIMK2 in *Nf2*$^{\Delta Ex2}$ MSCs confirmed the specificity of BMS-5 on LIMK activity. Intriguingly, during LIMK silencing in *Nf2*$^{\Delta Ex2}$ MSCs, we found that these cells did not sustain long-term LIMK knockdown and were able to restore their original expression levels. Thus, we only used cells within their first two passages after puromycin selection. We speculate that *Nf2*$^{\Delta Ex2}$ MSCs silence LIMK shRNA by a methylation-dependent mechanism as shown for PAK shRNAs in schwannoma cells [15].

Inhibition of LIMK activity with BMS-5 reduced *Nf2*$^{\Delta Ex2}$ MSCs viability by causing their arrest at the M phase of the cell cycle. Others have shown that LIMK's localization and activity changes during the cell cycle and that cofilin phosphorylation dynamics are necessary for successful cytokinesis [21, 23, 24]. Importantly, LIMK1 knockdown in HeLa cells or treatment with a LIMK inhibitor peptide resulted in delayed mitotic progression and irregular spindle orientation [22]. These reports support our conclusion that inhibition of LIMK activity with BMS-5 arrested *Nf2*-deficient cells in the M phase thereby decreasing the number of cells in S phase, and increasing the number of polyploid cells.

The reported interaction and functional cooperation of LIMK1 and 2 with Aurora A led us to explore the effect of LIMK inhibition with BMS-5 on Aurora A autophosphorylation[25]. In agreement with the observations made with LIMK1 knockdown in PC-3 cells, we found that BMS-5 reduced Aurora A phosphorylation at Thr288 (ref. 27). It is important to note that BMS-5 does not directly inhibit Aurora A kinase activity, because BMS-5 (compound 3 in ref. 35) was tested *in vitro* against a panel of kinases and Aurora A retained 100% activity when tested with 10 μM BMS-5 (ref. 35). Interestingly, the abnormal spindle and centrosome organization observed here resembles the abnormal metaphase spindles with multipolar and/or wheel-barrel shape and non-assembled chromosomes observed in a LIMK2 knockdown in SH-EP neuroblastoma cells [24]. The integrity of the mitotic spindle is required for progression from metaphase to anaphase, and any abnormality in the spindle assembly checkpoint delays or hinders the onset of anaphase. Hence, inhibition of LIMKs

activity by BMS-5 leads to inhibition of Aurora A kinase activity, and thus provides a molecular pathway for the G_2/M block of merlin deficient SCs treated with BMS-5.

Recently, LIMK has been show to promote tumor neovascularization through the VEGF/p38/MK2/LIMK1/annexin1 pathway [40]. This finding may potentially connect LIMK inhibition with the observed reduction in angiogenesis *in vivo* following treatment with Bevacizumab, which reduces tumor volumes and, in some patients, restores some hearing [4]. Thus, we speculate that inhibition of LIMK might halt tumor progression not only by interfering with cell-cycle progression in schwannoma cells, but also by inhibiting angiogenesis.

In conclusion, our studies suggest a potential therapeutic target for NF2, the LIMKs, which are recognized substrates of Cdc42/Rac-PAK1,2,4. We show enhanced LIMK expression and activity in merlin-deficient MSCs and as well as VS as opposed to controls. Reduction in LIMK activity or protein levels decreases *Nf2*-deficient MSC viability by arresting cells in the prometaphase stage of the cell-cycle in association with decreased activation of Aurora A necessary for centrosome and mitotic spindle organization. Future studies addressing whether LIMK inhibition is an effective treatment for schwannomas in mouse models of NF2 are warranted.

Materials and methods

Inhibitors

LIMK1/2 inhibitor, BMS-5 (CAS name N-(5–(192,6-dichlorophenyl)-3-(difluoromethyl)-1H-pyrazol-5-yl)thiazol-2-yl)isobutyramide) was from SynKinase (Shanghai, China). Rapamycin and staurosporine were from Santa Cruz Biotechnology (Santa Cruz, CA, USA).

Antibodies

Antibodies used were purchased from the following sources: phospho-Cofilin Ser3 (77G2), Merlin (D1D8), phospho-LIMK1(Thr508)/LIMK2(Thr505) (used in cell lines), LIMK1, phospho-Histone3(Ser10) (D2C8), α-Tubulin (DM1A), phospho-AuroraA(Thr288) (D13A11) and β-Actin (8H10D10) from Cell Signaling (Danvers, MA, USA); LIMK1 (clone42) mouse monoclonal antibody from BD Biosciences (San Jose, CA, USA); LIMK2, phospho-LIMK1 (pThr-508), and phospho-LIMK2 (pThr-505) rabbit antibodies from Sigma-Aldrich (St. Louis, MO, USA); S-100 rabbit antibody from Dako Cytomation (Glostrup, Denmark); Cofilin rabbit antibody from Novus Biologicals (Littleton, CO, USA);Centrin-1 rabbit antibody from Abcam (Cambridge, MA, USA); Aurora A rabbit antibody from Bethyl Laboratories (Montgomery, TX, USA); Peroxidase-conjugated goat anti-rabbit-IgG from Pierce, Thermo Fisher Scientific (Rockford, IL, USA); Highly cross-adsorbed Alexa Fluor® 488 goat anti-rabbit IgG (H+L) antibody from Invitrogen (Grand Island, NY, USA).

Generation of Nf2$^{\Delta Ex2}$MSCs

Nf2$^{\Delta Ex2}$ MSCs were generated *in vitro* by transducing *Nf2*$^{flox2/flox2}$ Schwann cells with an Adeno-Cre virus (University of Iowa Gene Transfer Vector Core) as previously described [41]. The *Nf2*$^{\Delta Ex2}$ MSCs were used up to passage 20. All protocols are in accordance with guidelines of and approved by the AAALAC International-certified UCF Institutional Animal Care and Use Committee.

Human Schwann cell cultures

Vials of frozen purified human SCs received from Dr. Patrick Wood at the University of Miami School of Medicine (Miami, FL, USA) were thawed and cultured on Corning dishes coated with 200 μg/ml poly-L-lysine (PLL) hydrobromide (Sigma-Aldrich) and 50 μg/ml Laminin (Invitrogen) containing D10M growth media: DMEM (Gibco) plus 10% heat inactivated fetal bovine serum (HIFBS) (HyClone, Logan, UT, USA), 2 μM Forskolin (Sigma), 0.02 mg/ml Pituitary Extract (Biomedical Tech. Inc) and 1% Penicillin/ Streptomycin (Gibco). Frozen vials from the stock bank of HSC were prepared by the Life Alliance Organ Recovery Agency at the University of Miami School of Medicine and cannot be traced to the specific donor. HSC were prepared from 10 cm biopsy of sural nerve/cauda equine from cadaveric adult human donors. Nerve fragments were incubated several days, dissociated and plated. SCs were purified by immunopanning with NGFR p75 antibodies. Culture purity based on S100 immunostaining was 96-99%. HEI-193 cells were purchased from ATCC (Manassas, VA, USA) and grown in DMEM plus 10% HIFBS and 1% Penicillin/Streptomycin.

Human Schwannoma samples

Frozen specimens of human sporadic vestibular schwannomas with different types of *NF2* mutations were procured with patient informed consents at The Ohio State University according to Institutional Review Board regulations.

Western blot analysis

Cultured cells were lysed in modified RIPA buffer (25 mM Tris-HCl pH 7.6; 150 mM NaCl: 1% Triton X-100, 1% Sodium dodecyl sulfate with protease inhibitor cocktail and phosphatase inhibitor cocktails 2 and 3, Sigma-Aldrich). VS specimens (0.1–0.2 gr) were homogenated in 900 μl of modified RIPA buffer with 25–30 strokes in a Wheaton Micro Tissue Grinder glass set # 528 (Wheaton Scientific, Millville, NJ, USA) on ice. Lysates were rotated for 10 min at 4°C and centrifuged for 10 min at 4°C, 15 000 rpm. Protein concentration was determined by DC Assay (BioRad, Hercules, CA, USA), and 10–20 μg of protein in Lamelli Buffer was resolved in 10% or 4–20% polyacrylamide gels (Pierce/Fisher Scientific), transferred to PVDF membrane (Immobilon-P, Millipore, Bedford, MA) and analyzed by western blotting with anti-LIMK1, (1:500) from BD for human samples and (1:500) from Cell Signaling for mouse samples, LIMK2 (1:500), P-cofilin-Ser3 (1:1 500), cofilin (1:70 000), merlin (1:500), S-100 (1:300), P-LIMK1-Thr508 (1:1 000), P-LIMK2-Thr505 (1:1 000), P-LIMK1(Thr508)/LIMK2(Thr505) (1:200) used in mouse and HEI193 cell lines, P-Aurora (1:1 000), AuroraA (1:500) and β-Actin (1:15 000) followed by corresponding secondary antibodies (1:20 000). Western blots were quantified by

densitometry using NIH ImageJ software. Intensities were normalized to β-actin loading controls.

LIMK1 and LIMK2 knockdown in Nf2$^{\Delta Ex2}$MSCs

Nf2$^{\Delta Ex2}$ MSCs were plated onto PLL-coated (200 μg/ml) 6-well dishes, cultured at 37°C, 7% CO_2, in medium containing DMEM/F12 (Invitrogen/Life Technologies, Grand Island, NY, USA) plus N2 supplement (Invitrogen: Burlington, ONT, Canada) and 1% Penicillin/Streptomycin. When cultures reached 40% confluence, lentiviral transduction particles were added at 5 multiplicity of infection (MOI) in growth medium plus 8 μg/ml hexadimethrine bromide (Sigma). MISSION shRNA lentiviral particles for mouse gene silencing were from Sigma-Aldrich. LIMK1 clone IDs: NM_010717.1-1546s1c1 (named construct #44); NM_010717.1-1414s1c1 (#47) and LIMK2 clone IDs: NM_010718.1-1409s1c1 (#73); NM_010718.3-827s21c1 (#95). Negative control was pLKO.1-puro non-mammalian shRNA (SHC002V). Optimum MOI determined empirically with pLKO.1-puro-CMV-TurboGFP transduction lentiviral particles (SHC003V) titer. After 18–20 hours, infection medium was replaced with fresh medium for 24 hours and subsequently replaced with growth medium containing 1μg/ml puromycin (Sigma-Aldrich) to select transduced cells. The puromycin concentration was determined performing a toxicity curve.

Reintroduction of NF2 into Nf2$^{\Delta Ex2}$MSCs

To reintroduce merlin into *Nf2*$^{\Delta Ex2}$ MSCs, 1.5–2 million cells were resuspended in 100 μl of basic Nucleofector solution for mammalian glial cells with supplements (Lonza, Cologne, Germany) plus 1 μg of pFC15K HaloTagCMVd1-*NF2* using an Amaxa Nucleofector II device and Program A-033. 1 ml of warm growth medium was added and 50 μl of cell suspension was seeded on coated 11mm round German glass coverslips (Carolina Biol., Burlington, NC, USA) containing 100 μl of equilibrated growth medium and incubated 40 hours at 37°C, 7% CO_2 before analysis.

Immunofluorescence

Cells were plated on coated German glass coverslips and immunostained as previously described [41]. Labeling of Halo-Tag-NF2-transfected cells was done *in vivo* with HaloTag® TMR Ligand (Promega, Madison, WI, USA) following manufacturer's rapid labeling protocol. Confocal images were acquired with a Zeiss LSM710 microscope with 3 spectral detection channels, 5 laser lines - 458, 488, 514,543 & 633 nm, FL filter set 49 DAPI, EX G365 shift free, FL filter set 43 CY 3 shift free, FL filter set 38 Endow GFP, shift free, Plan-Apochromat 63x/1.40 Oil DIC M27 and EC Plan-Neofluar 40x/1.3 DIC WD=0.21 M27 objective lenses on an AxioObserver Z1 Stand and ZEN2009 software. Fluorescence was collected from a single plane on separate channels maintaining the same acquisition parameters for each labeled protein. Images from each experiment were processed identically with ZEN2011 software. For spindle images, Z-stacks were collected with the 63xOil objective and 3.5 zoom factor. 2-D images were obtained by median filter and maximum intensity projection with ZEN2011.

Cell viability assay

Cell viability was assessed by CellTiter-Fluor assay (Promega) following manufacturer's specifications. Cells were seeded in 384-well format, centrifuged 1 min at 500 rpm and incubated at 37°C, 7% CO_2. After cell attachment (2.5–3.5 hrs), 5 μl/well of compound/vehicle solution was added and plates were quick spinned and incubated for 24 hrs. Fluorescence was measured with a Synergy H1 Hybrid plate reader (BioTek, Winooski, VT, USA).

Caspase activity assay

Caspase activity was assessed by the Apo-ONE homogeneous Caspase-3/7 assay (Promega) following manufacturer's specifications. Fluorescence was measured with a plate reader.

Membrane asymmetry assay

Cell membrane asymmetry was measured with the Violet Ratiometric Membrane Asymmetry Probe/Dead Cell Apoptosis Kit (Invitrogen/Life Technologies). Cells were seeded in 200 μg/ml PLL-coated 6-well plates and incubated with BMS-5/vehicle for 24 hrs. Cell were harvested and assayed following manufacturer's instructions. Samples were analyzed on a BD Canto-II (Becton, Dickinson and Co, Franklin Lakes, NJ, USA) flow cytometer setting excitation and collection emission wavelength recommended by the manufacturer. The ratio parameter was established using BD FACSDiva™ 6.1.3 software as recommended by the manufacturer.

Proliferation assays

Cell proliferation was studied with two different techniques. $Nf2^{\Delta Ex2}$ MSCs seeded in a 24-well format, had cell numbers assessed with the Crystal Violet Assay as previously described (42). Absorbance at 595 nm was measured with a μQuant plate reader (BioTek).

Rate of DNA synthesis was evaluated at 24 hrs with the Click-iT EdU Microplate Assay (Invitrogen/ Life Technologies). The assay was carried out in 96- and 384-well plate formats following manufacturer's instructions without the Amplex® UltraRed amplification steps. DAPI stain was included in the wash after the reaction cocktail incubation step. Oregon green-488 and DAPI fluorescence was quantified by a plate reader.

Cell cycle analysis

The cell cycle was analyzed by flow cytometry with propidium iodine (PI) staining and BrdU/7AAD. 10^6 ethanol fixed cells were PI stained using 500 μl PI/RNase staining buffer (Beckton-Dickinson). Samples were examined on a BD Canto-II flow cytometer and histograms were analyzed using ModFit LT software (Verity Software House, Topsham, ME, USA). For each sample, 10 000 events were collected.

The BrdU/7AAD assay kit was from Beckton-Dickinson. Cells were seeded in 6-well plates and treated with inhibitor/vehicle overnight. Next day, cultures were incubated with 10 μM BrdU for 3 hrs, and the assay performed according to manufacturer's instruction. Samples were analyzed with a BD Canto-II flow cytometer using the BD FACSDiva™ 6.1.3

software. FlowJo software (Tree Star, Inc, Ashland, OR, USA) was used for analysis of acquired data.

Statistical analysis

GraphPad Prism version 5.0 for Windows (GraphPad, La Jolla, CA, USA) was used for statistical analysis and graph generation of experimental data from three independent experiments. Dose response experiments were analyzed by non-linear regression (four parameters). Statistical analysis is indicated for each experiment.

Supplementary Material

Refer to Web version on PubMed Central for supplementary material.

Acknowledgments

We thank Dr. Patrick Wood, The Miami Project to Cure Paralysis, Department of Neurological Surgery, University of Miami Miller School of Medicine, Miami, FL, USA for vials of cultured human Schwann cells, Dr. Maria Elisa Manetti for the Halo-tag *NF2* plasmid, Nicklaus Sparrow and Marga Bott for creation of the $Nf2^{\Delta Ex2}$ MSCs, and Rashell Hallford for animal husbandry. This work was supported in part by a DHHS/NIH award to C.F.V. (5R01DC10189) and A.P. is the recipient of a Young Investigator Award from the Children's Tumor Foundation.

References

1. Rouleau GA, Merel P, Lutchman M, Sanson M, Zucman J, Marineau C, et al. Alteration in a new gene encoding a putative membrane-organizing protein causes neuro-fibromatosis type 2. Nature. 1993; 363(6429):515–521. [PubMed: 8379998]
2. Asthagiri AR, Parry DM, Butman JA, Kim HJ, Tsilou ET, Zhuang Z, et al. Neurofibromatosis type 2. Lancet. 2009; 373(9679):1974–1986. [PubMed: 19476995]
3. Baser ME, De Rienzo A, Altomare D, Balsara BR, Hedrick NM, Gutmann DH, et al. Neurofibromatosis 2 and malignant mesothelioma. Neurology. [Case Reports Research Support, U.S. Gov't, P.H.S. 2002; 59(2):290–291.
4. Plotkin SR, Stemmer-Rachamimov AO, Barker FG 2nd, Halpin C, Padera TP, Tyrrell A, et al. Hearing improvement after bevacizumab in patients with neurofibromatosis type 2. N Engl J Med. 2009; 361(4):358–367. [PubMed: 19587327]
5. Kalamarides M, Acosta MT, Babovic-Vuksanovic D, Carpen O, Cichowski K, Evans DG, et al. Neurofibromatosis 2011: a report of the Children's Tumor Foundation annual meeting. Acta Neuropathol. 2012; 123(3):369–380. [PubMed: 22083253]
6. Li W, Cooper J, Karajannis MA, Giancotti FG. Merlin: a tumour suppressor with functions at the cell cortex and in the nucleus. EMBO Rep. 2012; 13(3):204–215. [PubMed: 22482125]
7. Stamenkovic I, Yu Q. Merlin, a "magic" linker between extracellular cues and intracellular signaling pathways that regulate cell motility, proliferation, and survival. Curr Protein Pept Sci. 2010; 11(6): 471–484. [PubMed: 20491622]
8. Pelton PD, Sherman LS, Rizvi TA, Marchionni MA, Wood P, Friedman RA, et al. Ruffling membrane, stress fiber, cell spreading and proliferation abnormalities in human Schwannoma cells. Oncogene. 1998; 17(17):2195–2209. [PubMed: 9811451]
9. Kissil JL, Johnson KC, Eckman MS, Jacks T. Merlin phosphorylation by p21-activated kinase 2 and effects of phosphorylation on merlin localization. The Journal of biological chemistry. 2002; 277(12):10394–10399. [PubMed: 11782491]
10. Shaw RJ, Paez JG, Curto M, Yaktine A, Pruitt WM, Saotome I, et al. The Nf2 tumor suppressor, merlin, functions in Rac-dependent signaling. Dev Cell. 2001; 1(1):63–72. [PubMed: 11703924]
11. Xiao GH, Beeser A, Chernoff J, Testa JR. p21-activated kinase links Rac/Cdc42 signaling to merlin. The Journal of biological chemistry. 2002; 277(2):883–886. [PubMed: 11719502]

12. Kissil JL, Wilker EW, Johnson KC, Eckman MS, Yaffe MB, Jacks T. Merlin, the product of the Nf2 tumor suppressor gene, is an inhibitor of the p21-activated kinase, Pak1. Mol Cell. 2003; 12(4):841–849. [PubMed: 14580336]
13. Nakai Y, Zheng Y, MacCollin M, Ratner N. Temporal control of Rac in Schwann cell-axon interaction is disrupted in NF2-mutant schwannoma cells. J Neurosci. 2006; 26(13):3390–3395. [PubMed: 16571745]
14. Thaxton C, Lopera J, Bott M, Fernandez-Valle C. Neuregulin and laminin stimulate phosphorylation of the NF2 tumor suppressor in Schwann cells by distinct protein kinase A and p21-activated kinase-dependent pathways. Oncogene. 2008; 27(19):2705–2715. [PubMed: 17998937]
15. Yi C, Wilker EW, Yaffe MB, Stemmer-Rachamimov A, Kissil JL. Validation of the p21-activated kinases as targets for inhibition in neurofibromatosis type 2. Cancer Res. 2008; 68(19):7932–7937. [PubMed: 18829550]
16. Manetti F. LIM kinases are attractive targets with many macromolecular partners and only a few small molecule regulators. Med Res Rev. 2011; 32(5):968–998. [PubMed: 22886629]
17. Yang N, Higuchi O, Ohashi K, Nagata K, Wada A, Kangawa K, et al. Cofilin phosphorylation by LIM-kinase 1 and its role in Rac-mediated actin reorganization. Nature. 1998; 393(6687):809–812. [PubMed: 9655398]
18. Goyal P, Pandey D, Behring A, Siess W. Inhibition of nuclear import of LIMK2 in endothelial cells by protein kinase C-dependent phosphorylation at Ser-283. The Journal of biological chemistry. 2005; 280(30):27569–27577. [PubMed: 15923181]
19. Scott RW, Olson MF. LIM kinases: function, regulation and association with human disease. J Mol Med (Berl). 2007; 85(6):555–568. [PubMed: 17294230]
20. Yokoo T, Toyoshima H, Miura M, Wang Y, Iida KT, Suzuki H, et al. p57Kip2 regulates actin dynamics by binding and translocating LIM-kinase 1 to the nucleus. The Journal of biological chemistry. 2003; 278(52):52919–52923. [PubMed: 14530263]
21. Amano T, Kaji N, Ohashi K, Mizuno K. Mitosis-specific activation of LIM motif-containing protein kinase and roles of cofilin phosphorylation and dephosphorylation in mitosis. The Journal of biological chemistry. 2002; 277(24):22093–22102. [PubMed: 11925442]
22. Kaji N, Muramoto A, Mizuno K. LIM kinase-mediated cofilin phosphorylation during mitosis is required for precise spindle positioning. The Journal of biological chemistry. [Research Support, Non-U.S. Gov't]. 2008; 283(8):4983–4992.
23. Sumi T, Hashigasako A, Matsumoto K, Nakamura T. Different activity regulation and subcellular localization of LIMK1 and LIMK2 during cell cycle transition. Experimental cell research. [Comparative Study Research Support, Non-U.S. Gov't]. 2006; 312(7):1021–1030.
24. Po'uha ST, Shum MS, Goebel A, Bernard O, Kavallaris M. LIM-kinase 2, a regulator of actin dynamics, is involved in mitotic spindle integrity and sensitivity to microtubule-destabilizing drugs. Oncogene. 2010; 29(4):597–607. [PubMed: 19881550]
25. Nikonova AS, Astsaturov I, Serebriiskii IG, Dunbrack RL Jr, Golemis EA. Aurora A kinase (AURKA) in normal and pathological cell division. Cellular and molecular life sciences : CMLS. [Research Support N.I.H., Extramural Research Support, Non-U.S. Gov't Review]. 2013; 70(4): 661–687.
26. Barr AR, Gergely F. Aurora-A: the maker and breaker of spindle poles. Journal of cell science. [Research Support, Non-U.S. Gov'tReview]. 2007; 120(Pt 17):2987–2996.
27. Ritchey L, Ottman R, Roumanos M, Chakrabarti R. A functional cooperativity between Aurora A kinase and LIM kinase1: implication in the mitotic process. Cell Cycle. [Research Support, N.I.H., Extramural Research Support, U.S. Gov't, Non-P.H.S.]. 2012; 11(2):296–309.
28. Johnson EO, Chang KH, Ghosh S, Venkatesh C, Giger K, Low PS, et al. LIMK2 is a crucial regulator and effector of Aurora-A-kinase-mediated malignancy. Journal of cell science. 2012; 125(Pt 5):1204–1216. [PubMed: 22492986]
29. Bagheri-Yarmand R, Mazumdar A, Sahin AA, Kumar R. LIM kinase 1 increases tumor metastasis of human breast cancer cells via regulation of the urokinase-type plasminogen activator system. Int J Cancer. 2006; 118(11):2703–2710. [PubMed: 16381000]

30. Horita Y, Ohashi K, Mukai M, Inoue M, Mizuno K. Suppression of the invasive capacity of rat ascites hepatoma cells by knockdown of Slingshot or LIM kinase. The Journal of biological chemistry. 2008; 283(10):6013–6021. [PubMed: 18171679]

31. Okamoto I, Pirker C, Bilban M, Berger W, Losert D, Marosi C, et al. Seven novel and stable translocations associated with oncogenic gene expression in malignant melanoma. Neoplasia. 2005; 7(4):303–311. [PubMed: 15967107]

32. McConnell BV, Koto K, Gutierrez-Hartmann A. Nuclear and cytoplasmic LIMK1 enhances human breast cancer progression. Mol Cancer. 2011; 10:75. [PubMed: 21682918]

33. Manetti F. Recent findings confirm LIM domain kinases as emerging target candidates for cancer therapy. Curr Cancer Drug Targets. 2012; 12(5):543–560. [PubMed: 22414009]

34. Giovannini M, Robanus-Maandag E, van der Valk M, Niwa-Kawakita M, Abramowski V, Goutebroze L, et al. Conditional biallelic Nf2 mutation in the mouse promotes manifestations of human neurofibromatosis type 2. Genes Dev. 2000; 14(13):1617–1630. [PubMed: 10887156]

35. Ross-Macdonald P, de Silva H, Guo Q, Xiao H, Hung CY, Penhallow B, et al. Identification of a nonkinase target mediating cytotoxicity of novel kinase inhibitors. Mol Cancer Ther. 2008; (11): 3490–3498. [PubMed: 19001433]

36. Hung G, Li X, Faudoa R, Xeu Z, Kluwe L, Rhim JS, et al. Establishment and characterization of a schwannoma cell line from a patient with neurofibromatosis 2. International journal of oncology. [Research Support, Non-U.S. Gov't Research Support, U.S. Gov't, Non-P.H.S.]. 2002; 20(3):475–482.

37. Arber S, Barbayannis FA, Hanser H, Schneider C, Stanyon CA, Bernard O, et al. Regulation of actin dynamics through phosphorylation of cofilin by LIM-kinase. Nature. 1998; 393(6687):805–809. [PubMed: 9655397]

38. Bashour AM, Meng JJ, Ip W, MacCollin M, Ratner N. The neurofibromatosis type 2 gene product, merlin, reverses the F-actin cytoskeletal defects in primary human Schwannoma cells. Molecular and cellular biology. 2002; 22(4):1150–1157. [PubMed: 11809806]

39. Sparrow N, Manetti ME, Bott M, Fabianac T, Petrilli A, Bates ML, et al. The actin-severing protein cofilin is downstream of neuregulin signaling and is essential for Schwann cell myelination. J Neurosci. 2012; 32(15):5284–5297. [PubMed: 22496574]

40. Cote MC, Lavoie JR, Houle F, Poirier A, Rousseau S, Huot J. Regulation of vascular endothelial growth factor-induced endothelial cell migration by LIM kinase 1-mediated phosphorylation of annexin 1. J Biol Chem. 2010; 285(11):8013–8021. [PubMed: 20061392]

41. Thaxton C, Bott M, Walker B, Sparrow NA, Lambert S, Fernandez-Valle C. Schwannomin/merlin promotes Schwann cell elongation and influences myelin segment length. Mol Cell Neurosci. 2011; 47(1):1–9. [PubMed: 21182951]

42. Iacovelli J, Lopera J, Bott M, Baldwin E, Khaled A, Uddin N, et al. Serum and forskolin cooperate to promote G1 progression in Schwann cells by differentially regulating cyclin D1, cyclin E1, and p27Kip expression. Glia. 2007; 55(16):1638–1647. [PubMed: 17849471]

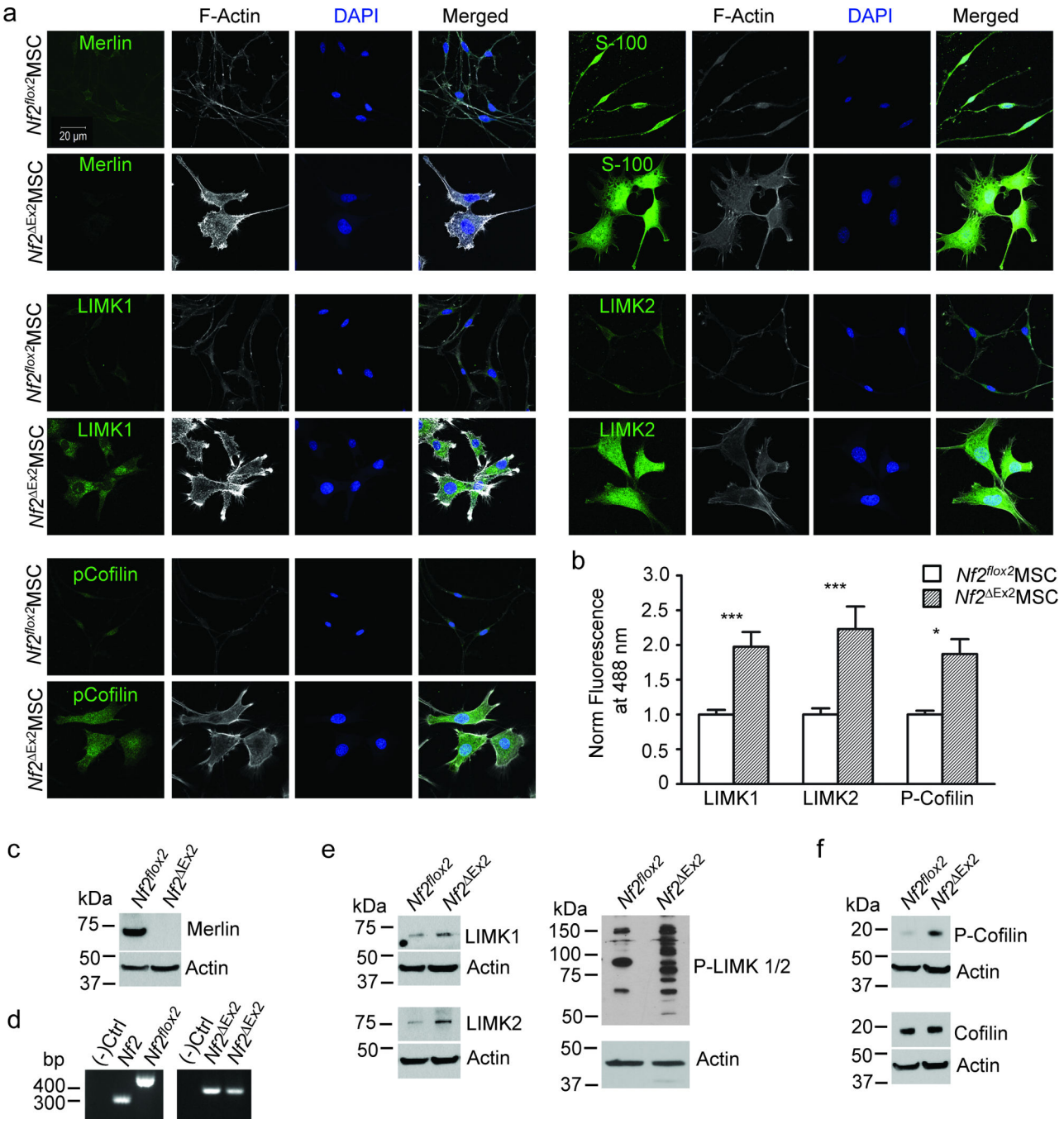

Figure 1. Elevated levels of LIMK and phospho-Ser3-cofilin in *Nf2*$^{\Delta Ex2}$ MSCs compared to control MSCs

(a) Representative confocal images of *Nf2*$^{\Delta Ex2}$ MSCs and *Nf2*$^{flox2/flox2}$ MSCs grown overnight on glass coverslips, fixed and immunostained with the indicated antibodies (green). F-actin was visualized with phaloidin-Alexa633 (white) and the nucleus was visualized by DAPI stain (blue). Scale bar: 20 μm. (**b**) Quantitation of the immunofluorescence for the indicated proteins in three independent experiments was performed with Volocity software. ***P<0.001; *P<0.05 determined by two-way ANOVA

using Bonferroni post-tests. **(c)** Characterization of $Nf2^{flox2/flox2}$ and $Nf2^{\Delta Ex2}$ MSCs. Control *Nf2* with the exon2 flanked by loxP sites, $Nf2^{flox2/flox2}$ and $Nf2^{\Delta Ex2}$ MSCs analyzed by western blotting for N-terminus merlin and **(d)** PCR analysis of genomic DNA. Primers P4/P5 amplified a 305-bp band for wild type *Nf2* FVB/N and a 442-bp band for $Nf2^{flox2/flox2}$ and primers P6/P5 amplified a 338-bp band for $Nf2^{\Delta Ex2}$. **(e)** $Nf2^{\Delta Ex2}$ MSCs and control $Nf2^{flox2/flox2}$ MSCs analyzed by western blotting for LIMK1, LIMK2, phospho-LIMK1/2 (Thr508/505), and **(f)** phospho-Ser3-cofilin and cofilin. Anti-β-actin was used as a loading control.

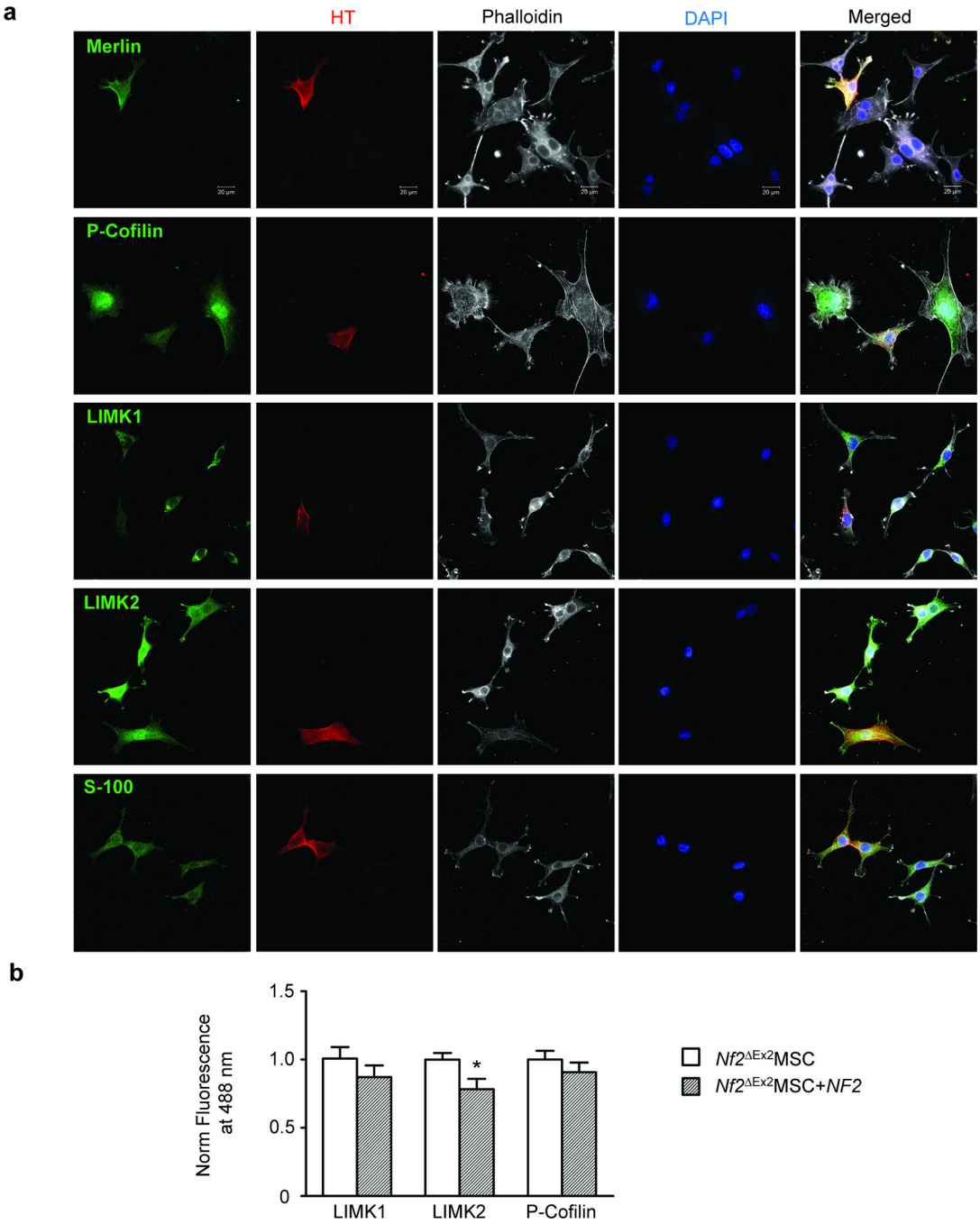

Figure 2. Reintroduction of wild-type merlin normalizes LIMK expression levels

(a) *Nf2*$^{\Delta Ex2}$ MSCs were transfected with Halo-tag-*NF2* and incubated for 40 hrs on glass coverslips coated with 200 μg/ml PLL and 10 μg/ml Laminin. Transfected cells were identified by halo-tag TMR labeling (red). Cells were fixed and immunostained for the indicated proteins (green). F-actin was visualized with phaloidin-Alexa633 (white) and the nucleus with DAPI (blue). Confocal images are representative of three independent experiments. Scale bar: 20 μm. **(b)** Quantitation of (a). Measurements of the mean pixel intensity fluorescence in the green channel of 2 experiments for the indicated proteins were

performed with Volocity software. *P<0.05 determined by two-way ANOVA using Bonferroni post-tests.

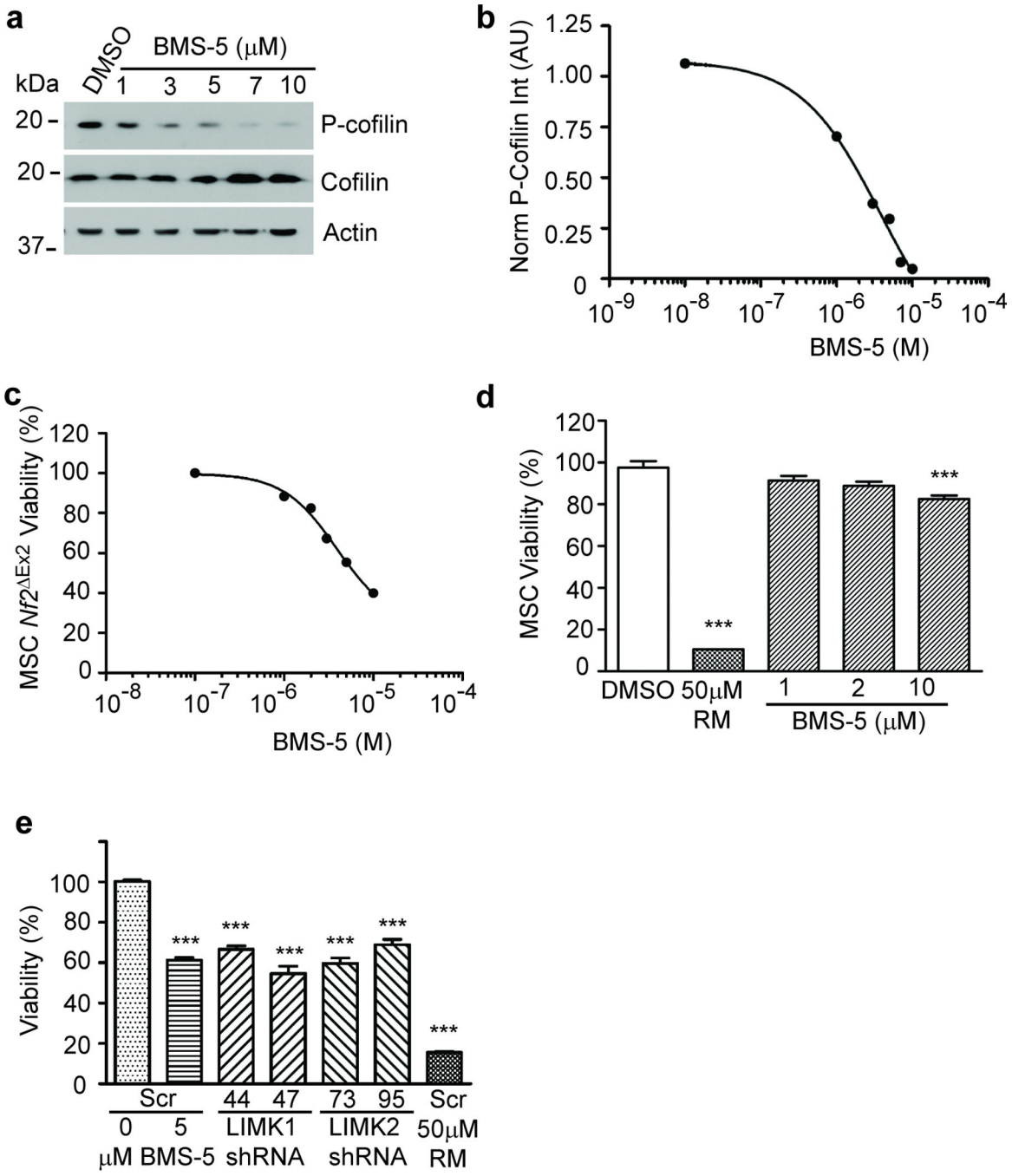

Figure 3.

LIMK inhibition by BMS-5 or silencing by shRNA in $Nf2^{\Delta Ex2}$ MSCs decreases cell viability. **(a)** BMS-5 dose-response western blot. $Nf2^{\Delta Ex2}$ MSCs were plated in 12-well plates. Cultures were treated the next day as indicated for 30 min. Cells were harvested, lysed and analyzed by western blotting for phospho-Ser3-cofilin and total cofilin. β-actin levels were used as loading controls for normalization. Representative blot of three independent experiments. **(b)** BMS-5 dose-response curve of cofilin phosphorylation in $Nf2^{\Delta Ex2}$ MSCs. Analyzed as log [inhibitor] vs. response, variable slope (four parameters).

(c) BMS-5 dose viability-response curve. *Nf2*$^{\Delta Ex2}$ MSCs were seeded at 5 000 cells/well in 20 μl growth medium phenol-red free in a 384-well plate and after attachment were incubated with BMS-5 for 24 hrs. Cell viability was measured with the CellTiter-Fluor assay. Graph represents the mean ± SEM of 3 independent experiments analyzed together (n=96) log [inhibitor] vs. response, variable slope (four parameters). **(d)** BMS-5 viability response of control MSCs. Cell viability was measured as in (c). Graph represents the mean ± SEM (n=16). DMSO control was considered 100% viability. Rapamycin (RM) (50 μM) was a positive control for cell death. ***P<0.001 determined by one-way ANOVA using Dunnett's multiple comparison test.

(e) Viability of *Nf2*$^{\Delta Ex2}$ MSCs expressing LIMK 1 or LIMK2 shRNAs were compared to cells expressing scrambled shRNA untreated or treated with 5 μM BMS-5 or 50 μM rapamycin (RM) for 24 hrs in a 384-well format. Cell viability was measured with the CellTiter-Fluor assay. *Nf2*$^{\Delta Ex2}$ MSCs expressing scrambled shRNA represented 100% viability, and the 50 μM RM treated cells were a positive control for cell death. Graph represents the mean ± SEM of 4 independent experiments analyzed together (n=128). ***P<0.001determined by one-way ANOVA using Dunnett's multiple comparison test

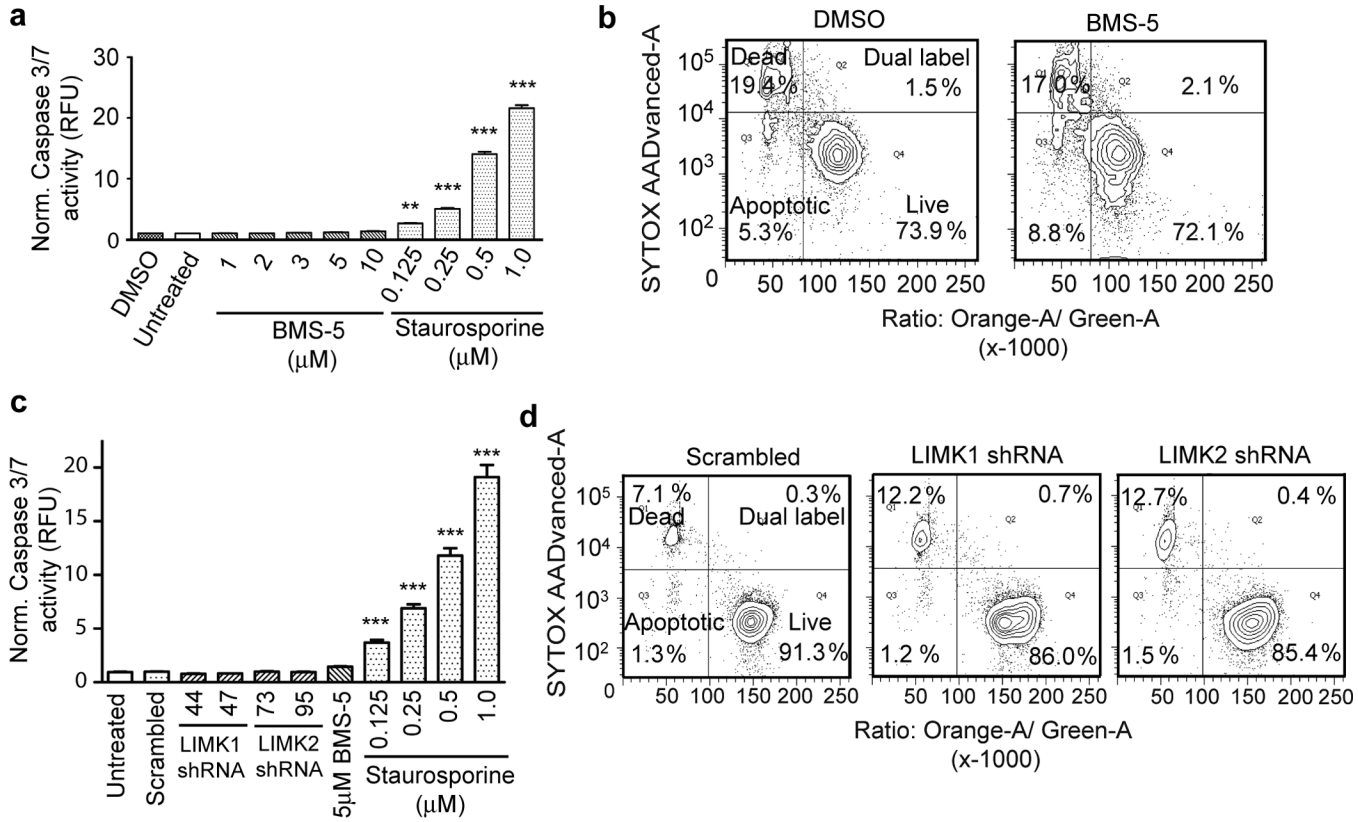

Figure 4.

Inhibition or silencing of LIMK does not induce apoptosis.**(a)** Caspase 3/7 activity assay. *Nf2*$^{\Delta Ex2}$ MSCs were seeded at 5 000 cells/well in 20 μl growth media, phenol-red free in a 384-well plate and incubated for 16 hrs at 37°C, 7% CO_2. Next, 5 μl/well of the indicated solution was added and incubated for 8 hrs. Caspase 3/7 activity was measured with the ApoONE Homogeneous assay. Staurosporine curve was used as positive control. Histogram represents 3 independent experiments (n=96) normalized to untreated and analyzed together. ***P*<0.01; ****P*<0.001 determined by one-way ANOVA using Dunnett's multiple comparison test. **(b)** *Nf2*$^{\Delta Ex2}$ MSCs plated in a 6-well format were incubated with 2 μM BMS-5 or DMSO vehicle for 24 hrs. Plasma membrane asymmetry was evaluated with the Violet ratiometric assay by flow cytometry. Densitometry graph illustrates the following quadrants: apoptotic (Q3), dead (Q1), live (Q4) and dual label (Q2). **(c)** Caspase 3/7 activity measured with the ApoONE assay of *Nf2*$^{\Delta Ex2}$ MSCs uninfected or infected with control scrambled or the indicated constructs for LIMK1/2 shRNA silencing. Cells were incubated 24 hrs in a 384-well format and in the presence of inhibitors for 8 hrs where indicated. Staurosporine response was used as positive control. Histogram represents 5 independent experiments normalized to scrambled control and analyzed together (n=160). ****P*<0.001 determined by one-way ANOVA using Dunnett's multiple comparison test. **(d)** *Nf2*$^{\Delta Ex2}$ MSCs infected with scrambled shRNA or shRNAs targeting LIMK1/2 constructs were plated in a 6-well format and incubated for 24 hrs. Plasma membrane asymmetry was assessed with the Violet ratiometric assay by flow cytometry in three independent

experiments. Densitometry plots show the quantification of the population distribution into the four quadrants as in (b).

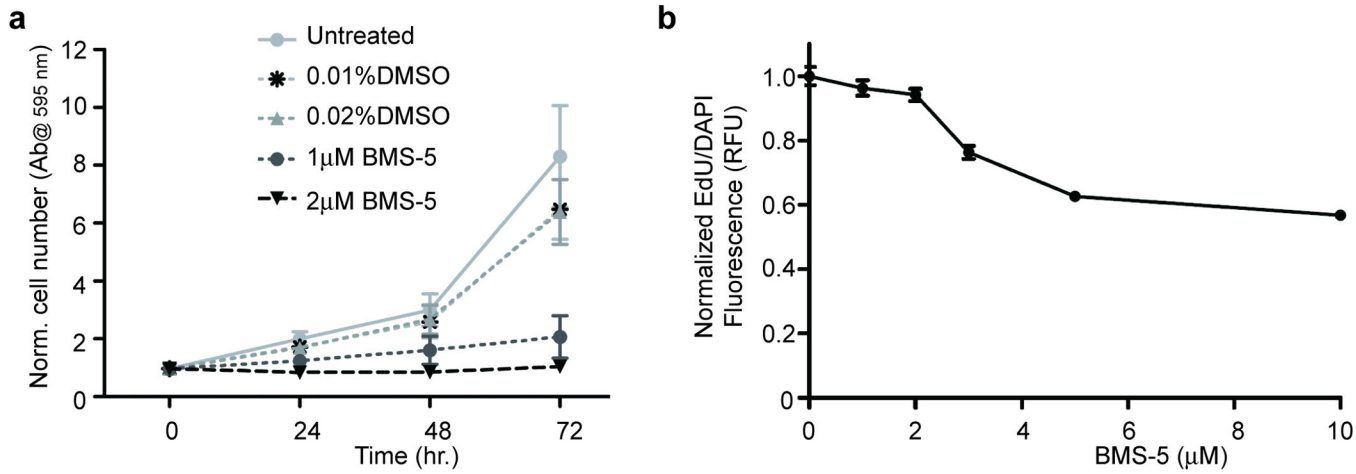

Figure 5.

BMS-5 decreases *Nf2*$^{\Delta Ex2}$ MSC proliferation and DNA synthesis in a dose-dependent manner. **(a)** *Nf2*$^{\Delta Ex2}$ MSCs were grown in 24-well plates. Cell proliferation was measured at 0; 24; 48 and 72 hrs time points after incubation with BMS-5 or DMSO vehicle. The number of cells at each time point was assessed with the crystal violet assay. Graph combines 3 independent experiments in triplicates (mean ± SEM, n=9). **(b)** *Nf2*$^{\Delta Ex2}$ MSCs were treated with the indicated BMS-5 concentrations for 24 hrs. EdU was added to the culture for the last 6 hours. Incorporation of EdU into S-phase cells was assessed with the EdU Click-It microplate assay and fluorescence was measured on a plate reader. Graph combines 3 independent experiments (mean ± SEM, n=44).

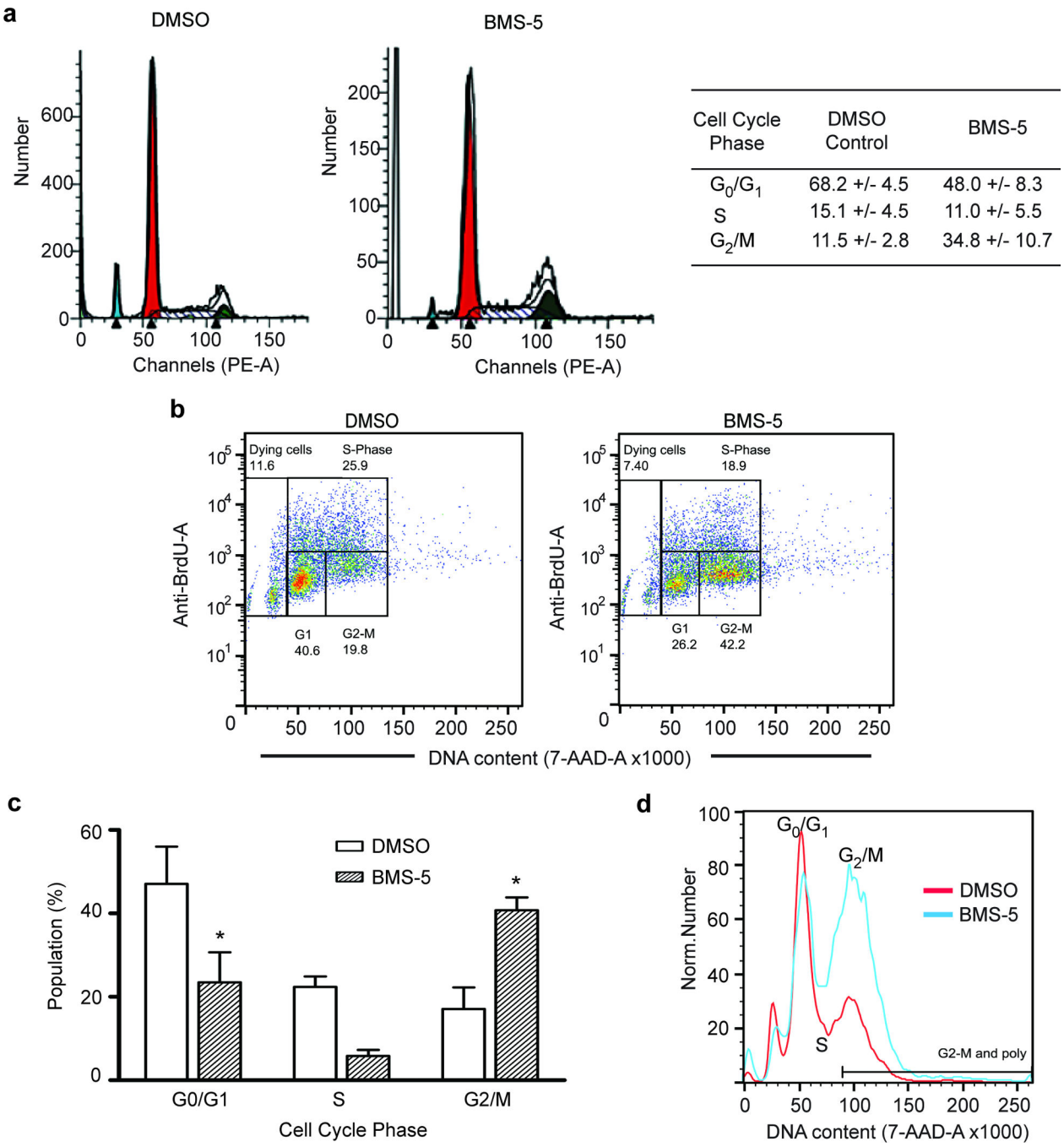

Cell Cycle Phase	DMSO Control	BMS-5
G_0/G_1	68.2 +/- 4.5	48.0 +/- 8.3
S	15.1 +/- 4.5	11.0 +/- 5.5
G_2/M	11.5 +/- 2.8	34.8 +/- 10.7

Figure 6.

Inhibition of LIMK interferes with cell cycle progression of $Nf2^{\Delta Ex2}$ MSCs. **(a)** $Nf2^{\Delta Ex2}$ MSCs were grown in a 6-well format and treated with 5 μM BMS-5 for 7 hours prior to labeling. Cells were analyzed by flow cytometry. Propidium iodide labeling profile of the diploid cell population analyzed with the ModFit program. Tabulation of the distribution of cell cycle phases of 3 independent experiments (mean± SEM, n=3). **(b)** $Nf2^{\Delta Ex2}$ MSCs were treated with 5 μM BMS-5 or DMSO control overnight prior to 3 hr BrdU labeling and analysis by flow cytometry. Distribution of BrdU- and 7-AAD-labelled cells analyzed with

FlowJo software. These distribution plots are representative of 4 independent experiments (n=4). **(c)** Graph of the distribution of the cell cycle phases of all the experiments as mean ± SEM, **P*<0.05 determined by two-way ANOVA and Bonferroni multiple comparisons post-test. **(d)** Overlay of histograms of 7-AAD content comparing the vehicle and BMS-5 treated cells shown in (b).

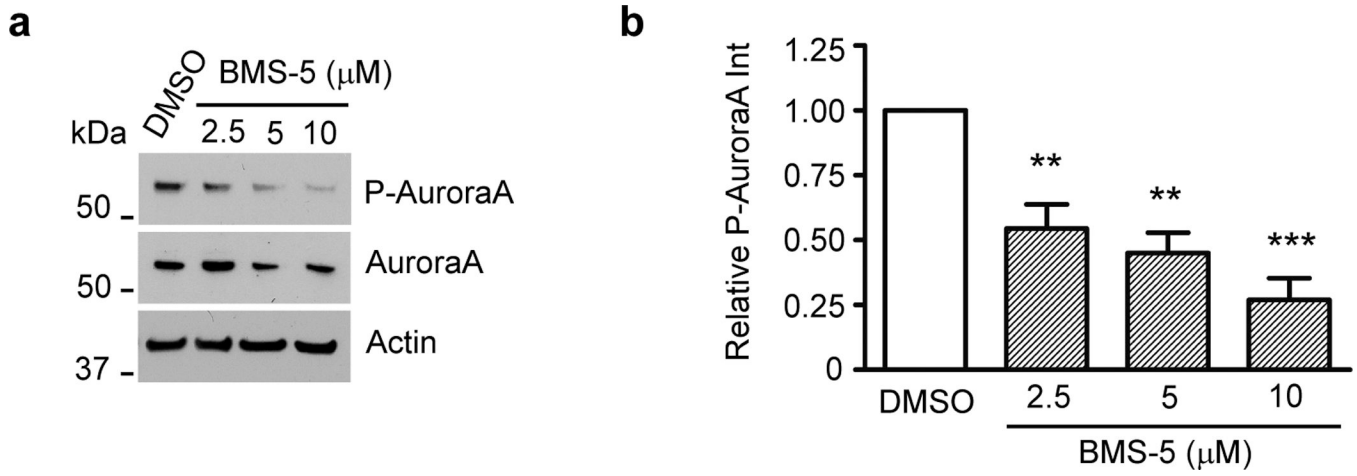

Figure 7.

Inhibition of LIMKs decreases Aurora A autophosphorylation. **(a)** Representative western blot of three independent BMS-5 dose-response experiments. *Nf2*$^{\Delta Ex2}$ MSCs were plated in half of a 12-well plate and treated the next day with increasing BMS-5 concentrations or DMSO for 8 hr. Cells were harvested, lysed and 10 μg of protein were analyzed by western blotting for phospho-Thr288-Aurora A and Aurora A. β-actin levels were used as loading controls. **(b)** Quantification of BMS-5 effect-response on Aurora A phosphorylation. Graph represents the mean ± SEM (n=3), ***P*<0.01; *** *P*<0.001 determined by one-way ANOVA using Dunnett's multiple comparison test.

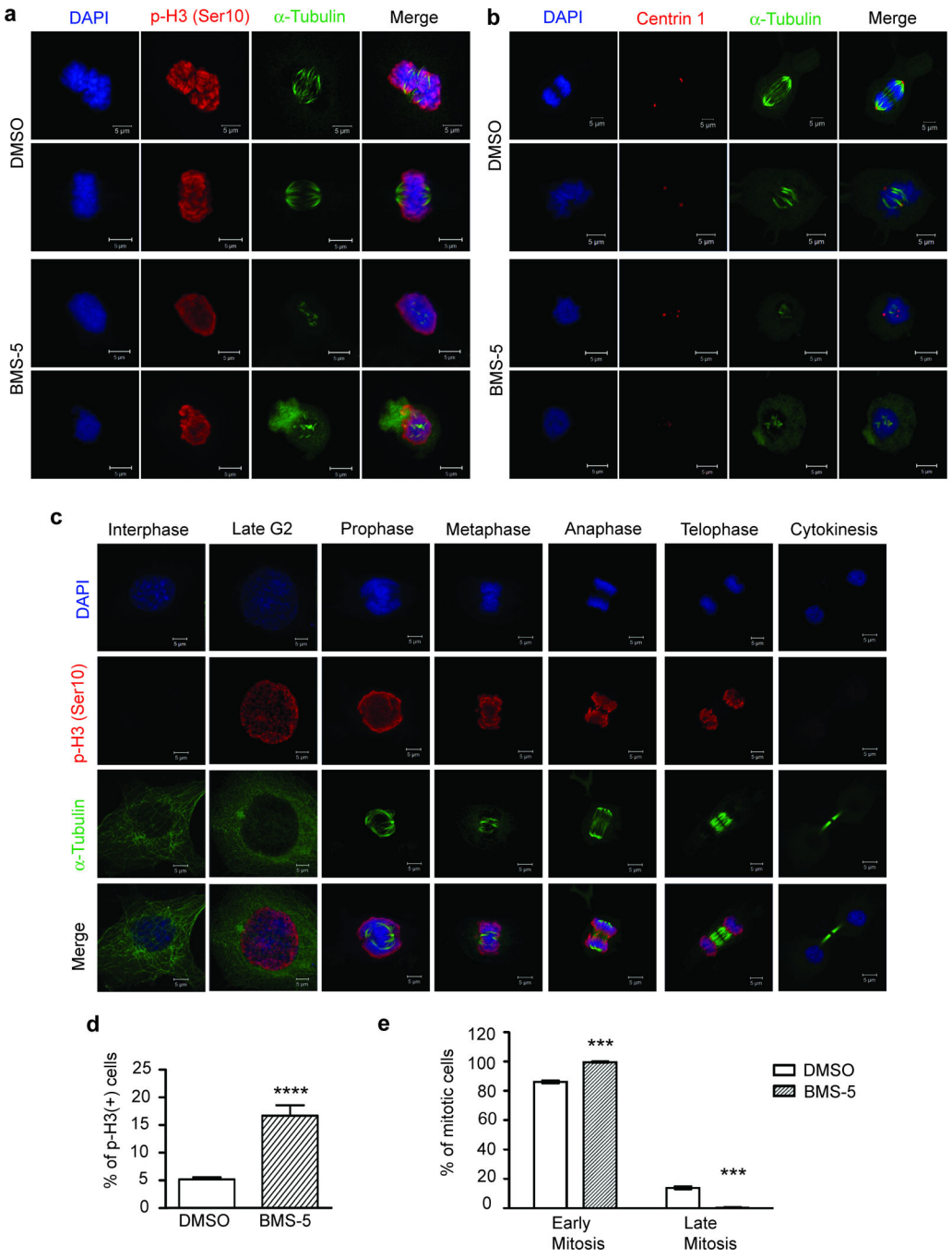

Figure 8.

Inhibition of LIMKs produce abnormal spindle and centrosome assemblies.**(c)** Representative confocal images of *Nf2*$^{\Delta Ex2}$ MSCs grown overnight on glass coverslips and treated with 4 μM BMS-5 or 0.04% DMSO for 8 hrs , fixed and immunostained with α-tubulin (green) and **(a)** P-H3(ser10) or **(b)** centrin1 (red). Nuclei were visualized with DAPI (blue).**(c)** Representative confocal images of DMSO treated *Nf2*$^{\Delta Ex2}$ MSCs depicting the cell cycle phases considered for analysis. **(d)** Quantification of the percentage of cells in late G_2/M phase assessed by positive p-H3 immunostaining. **** P<0.0001 determined by

unpaired t test, two-tailed, from triplicate coverslips of three independent experiments (n=9). **(e)** Quantification of the percentage of mitotic cells in early (pro/metaphase) and late (ana/telophase) mitosis. *** $P<0.001$ determined by two-way ANOVA and Bonferroni multiple comparisons post-test. Scale bar: 5 μm.

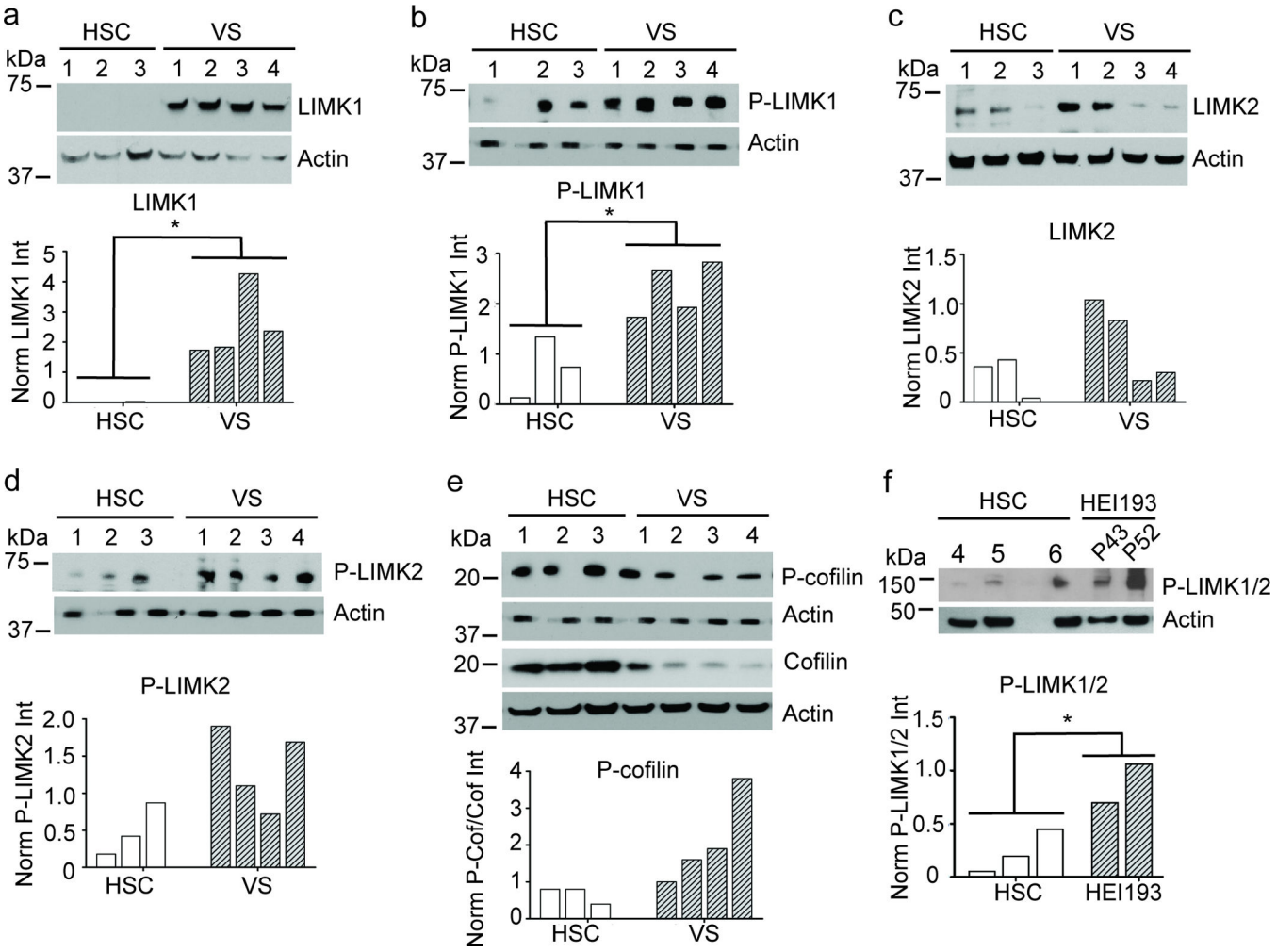

Figure 9.

LIMKs are overexpressed in human vestibular schwannomas. Lysed cultured human Schwann cells (HSC) cultured in 100-mm dishes and homogenized frozen human sporadic vestibular schwannomas (VS) were resolved by SDS-PAGE and analyzed by western blot. Quantitation of the western blots was done by densitometry analysis with ImageJ software, normalized to β-actin and is plotted below. Western blots for **(a)** LIMK1, **(b)** phospho-Thr508-LIMK1, **(c)** LIMK2, **(d)** phospho-Thr505-LIMK2 and **(e)** phospho-Ser3-cofilin and cofilin. β-actin was used as a loading control. **P*<0.05 determined using unpaired *t*-test of HSC vs. VS populations, two-tailed. **(f)** HSCs from normal individuals (control) and HEI193 cells at P43 and P52 were cultured in 60-mm dishes and analyzed by western blotting for phospho-Thr508/505-LIMK1/2. β-actin was used as a loading control.